Modular Arbitrary Waveform Dielectric Spectrometer for Aging Diagnostics of Recessed Specimens

Author(s):
Färber, Raphael; Franck, Christian

Publication date:
2016

Permanent link:
https://doi.org/10.3929/ethz-b-000123383

Originally published in:
https://doi.org/10.1109/CEIDP.2016.7785614

High Voltage Laboratory

Modular Arbitrary Waveform Dielectric Spectrometer for Aging Diagnostics of Recessed Specimens

R. Faerber
C. M. Franck

This article was presented at the *Conference on Electrical Insulation and Dielectric Phenomena (CEIDP)*, 2016. Toronto.

ETH
Eidgenössische Technische Hochschule Zürich
Swiss Federal Institute of Technology Zurich

Modular Arbitrary Waveform Dielectric Spectrometer for Aging Diagnostics of Recessed Specimens

R. Faerber, C. M. Franck
High Voltage Laboratory, ETH Zürich, Physikstrasse 3, 8092 Zürich

***Abstract*- The advent of solid-state switches with blocking voltages in excess of 10 kV and new medium-voltage multi-level converter topologies raise issues with respect to the long-term endurance of the high voltage insulation systems exposed to the high-frequency pulse-shaped voltage stresses. In this paper we present a modular dielectric spectrometer specifically designed for aging studies on recessed polymeric specimens. Its aim is to quantify the pre-breakdown degradation caused by repetitive pulsed high-voltage stresses by using the complex dielectric permittivity as an aging marker. Moreover, its ability to operate with multi-frequency excitation voltages allows investigations on the possibility of using dielectric spectroscopy as an online monitoring tool for insulation systems exposed to the mentioned stresses.**

In this contribution a detailed description of the setup and a characterization of its accuracy and precision for sinusoidal excitations is given. It is shown that despite the small specimen capacitances of a few pF, the loss factor can be resolved with a precision $\leq 10^{-4}$ for frequencies ranging from 10 Hz up to 600 kHz.

I. Introduction

The recent developments in silicon carbide (SiC) solid-state switches open up new possibilities in medium-voltage (MV) power electronic converter design and applications [1]. In addition to established semiconductor-based grid technologies such as High-Voltage DC (HVDC) and Flexible AC Transmission Systems (FACTS) [2], intensive research and development on new devices such as MV Solid-State Transformers (SSTs) [3] is currently going on. They represent promising alternatives to conventional low-frequency MV transformers in certain applications. In addition to exhibiting higher power densities, they excel through their unprecedented flexibility in electrical power conversion and conditioning (*active* grid-grid, grid-load or grid-source interfaces linking different voltage and/or frequency levels, including DC).

With newly available SiC switches featuring blocking voltages in excess of 10 kV and usable switching frequencies of several tens of kilohertz, high voltage engineering will inevitably face new challenges concerning the endurance of insulation systems exposed to these non-harmonic, high-frequency high-voltage stresses [4]. Whether it be through single-stage or cascaded medium-voltage converter topologies, certain parts of the insulation system (e.g. the winding insulation in the medium-frequency transformer of an SST) will be exposed to both high voltages (>10 kV) and high slew rates (>10 kV/µs) with high repetition frequencies. Corresponding two- or multilevel Pulse-Width-Modulated (PWM) MV waveforms have been shown to lead to enhanced partial discharge activity and corresponding accelerated aging of wire insulation in inverter-fed induction motors [5] as well as to reduced breakdown voltages of oil-impregnated paper insulation [6].

Apart from enhanced dielectric heating due to the presence of harmonics [7] the degradation processes in dry-type insulation materials active under this type of field stress *below partial discharge inception* are not well explored. Information about these degradation mechanisms is however needed for the development of insulation concepts that ensure insulation endurance over the intended system lifetime.

In addition to being promoted to a design criterion in broadband applications, the frequency (and temperature) dependence of the complex dielectric permittivity is a promising aging marker, as stress-induced microscopic changes in the molecular structure of the insulation material preceding its breakdown may be reflected therein. Its potential is further strengthened by its *relative* ease of access (through a *precise* impedance measurement) and the presence of a (controllable) broadband voltage excitation in converters. The former makes it a candidate for online monitoring applications while the latter allows the use of Arbitrary Waveform Impedance Spectroscopy (AWIS) [8].

In order to explore the above-mentioned potentialities, the modular arbitrary waveform dielectric spectrometer presented in this paper has been built. It allows multifactorial aging studies on recessed specimens (stressing is done in a dedicated MV test bench) for which the parasitic deteriorating influence of partial discharges in the ambient medium of parallel plate specimens are absent. These samples typically have capacitance values between 1 pF and 5 pF for which general-purpose table-top impedance analyzers perform poorly while dedicated turnkey solutions are very costly. Finally, commercially available test fixtures for bulk material characterization are intended for disc-shaped specimens while the test cell presented here accommodates both specimen geometries in a guarded three-electrode arrangement.

The aim of the developed research setup is twofold. Firstly, it shall be used as a diagnostic tool on the recessed specimens for assessing the usability of the dielectric permittivity as an aging marker for insulation materials exposed to PWM-type high-voltage stress. Secondly, its modular makeup is intended to provide the necessary flexibility for exploring various approaches of extending offline (arbitrary waveform) spectroscopy to an online monitoring setup allowing real-time monitoring of dielectric properties under PWM high-voltage stress.

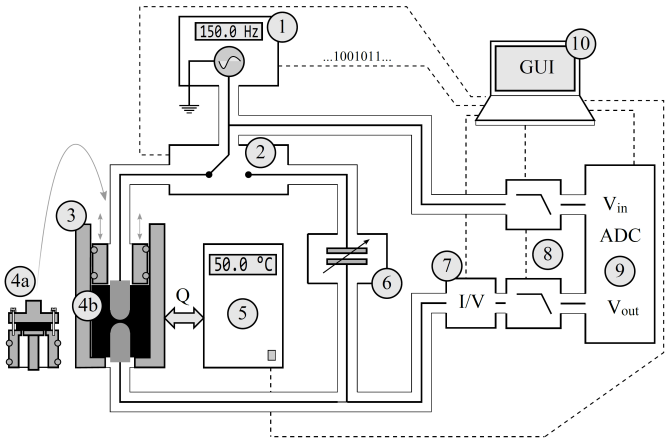

Fig. 1. Schematic of the modular dielectric spectrometer. The labels are referred to in the main text. ④a is a parallel-plate sample holder which can be inserted into the test cell in place of the recessed specimen ④b.

After a detailed description of the experimental setup (section II), benchmark tests regarding accuracy and precision are presented (sections III.A/B). The influence of specimen geometry and system nonlinearities on measured parameters are presented in sections III.C/D, respectively. The results are discussed in section IV and a conclusion with a short outlook on future research is given in section V.

II. Experimental Setup

A. Dielectric Spectrometer

A schematic of the setup is shown in Fig. 1. A periodic voltage excitation $V_{in}(t) = V_{in}(t + 1/f_0)$ with spectral content $\underline{V}_{in}(\omega)$ and a maximal amplitude of 20 V_{pp} is generated by an arbitrary function generator ① (Agilent 33210A). The signal lines are coaxially shielded throughout the analog stage. The current $\underline{I}_{out}(\omega)$ excited in the measurement electrode (see section II.C) by the impressed voltage is amplified and converted into a voltage $\underline{V}_{out}(\omega) = \underline{\alpha}(\omega)\underline{I}_{out}(\omega)$ by a low-noise transimpedance amplifier ⑦ (FEMTO DLPCA-200). The magnitude of the transimpedance gain $\underline{\alpha}$ is variable between 10^3 and 10^9 V/A, with a -3 dB low-pass cutoff frequency decreasing from 500 kHz below 10^4 V/A to 1.1 kHz at the highest gain.

The voltages $\underline{V}_{in}$ and $\underline{V}_{out}$ can be low-pass filtered ⑧ to avoid aliasing when they are digitized by the 16-bit 1 MHz simultaneous analog-to-digital converter (ADC) ⑨ (NI 9223). Vertical resolution (dynamic range) is particularly important for AWIS, where frequency components differing by two or more orders of magnitude are captured simultaneously. The used ADC has an analog bandwidth >1 MHz which allows using a simple undersampling technique on the repetitive analog signals, extending the virtual sampling frequency on periodic signals up to ~50 MHz and the *phase-sensitive* measurement of voltages up to ~1 MHz with 16-bit precision. The fundamental excitation frequency f_0 is fine-tuned such that with the exactly available sampling frequencies f_s of the ADC one has $m/f_0=n/f_s$, where n and m are positive integers (coherent sampling). This allows using rectangular windowing for the Discrete Fourier Transform (DFT) without spectral leakage. In the undersampling mode one chooses in addition $n=2^q$ with integer q and $m>2$ prime such that m signal periods are sampled at 2^q non-equivalent phase positions. The sampled points are then reduced to a single period virtually sampled at $m{\cdot}f_s$.

In the results presented here single periods were measured (i.e. $m=1$ in the absence of undersampling) and their discrete spectral content $\underline{V}_{in,i}(\omega_k)$ and $\underline{V}_{out,i}(\omega_k)$ with $\omega_k = 2\pi k f_0$ determined by a Fast Fourier Transform up to the Nyquist frequency. The index i enumerates the outcomes of N such measurements.

The complex relative permittivity $\underline{\varepsilon}(\omega_k) = \varepsilon'(\omega_k) - j\varepsilon''(\omega_k)$ is related to the measured impedance $\underline{Z}(\omega_k)$ by

$$\underline{\varepsilon}(\omega_k) = \left[j\omega_k C_{0,S}\underline{Z}(\omega_k)\right]^{-1} \tag{1}$$

where $C_{0,S}$ designates the vacuum capacitance of the specimen. The impedance is given by

$$\underline{Z}(\omega_k) = \frac{\underline{\beta}_{in}(\omega_k)\underline{V}_{in}(\omega_k)}{\underline{\beta}_{out}(\omega_k)\underline{V}_{out}(\omega_k)} \tag{2}$$

where the $\underline{\beta}$ factors account for all *linear* transfers (e.g. the transimpedance gain) in the signal chain. For each excitation frequency a switch ② (Agilent 8762A) alternately selects between the sample path and a reference path containing an air capacitor ⑥ of capacitance $C_{0,R} \approx C_{0,S} \cdot \left|\underline{\varepsilon}(f = 1\text{kHz})\right|$ for which the complex relative permittivity is equal to ~1. Assuming the transfer coefficients to be the same for signal and reference measurements allows eliminating the latter and expressing the permittivity in terms of measured voltages and vacuum capacitances. The reported permittivity is the arithmetic mean of measurements i=1,…,*N*,

$$\underline{\varepsilon}(\omega_k) = \frac{C_{0,R}}{C_{0,S}} N^{-1} \sum_{i=1}^{N} \frac{\underline{V}_{out,i,S}(\omega_k)\underline{V}_{in,i,R}(\omega_k)}{\underline{V}_{in,i,S}(\omega_k)\underline{V}_{out,i,R}(\omega_k)}. \tag{3}$$

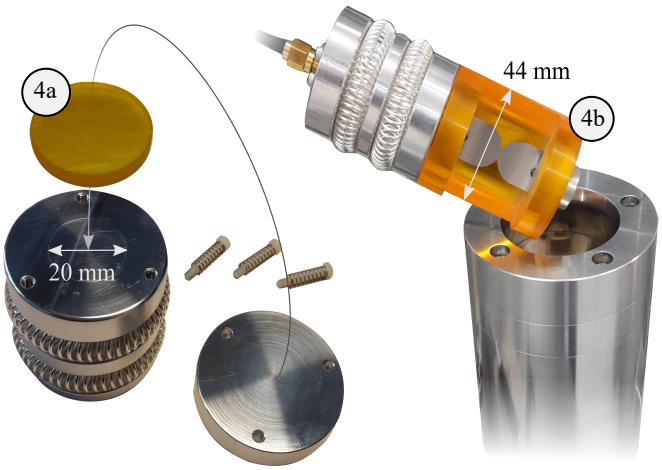

Fig. 2. Guarded parallel-plate sample holder for disc-shaped specimens (left) and recessed specimen (electrodes exposed for viewing purposes) being mounted into the test cell (right).

One notes that there is no need for the N measurements to be triggered at the same phase angle. Error bars are α=0.95 confidence intervals for the arithmetic mean constructed from Student's t coefficient and the sample standard deviation S_N of the measured quantity ($\pm t_{\alpha,N-1} N^{-0.5} S_N$). Henceforth, "significantly different" will be used to designate measurements with non-overlapping confidence intervals.

The permittivity is thus obtained for all Fourier components contained in the digitized signal. In practice, the usability of a specific frequency value depends on the magnitude of the corresponding Fourier amplitude with respect to the noise floor of the system. For the results reported in this paper, only sinusoidal excitations were used and accordingly only $\underline{\varepsilon}(\omega_1)$ available as an output of the measurement.

The value $C_{0,S}$ of the recessed specimen ④b is determined by imposing the value of the permittivity at a certain frequency and temperature (e.g. 1 kHz, 20 °C), previously determined for the corresponding material in parallel plate geometry ④a under the same conditions (e.g. after drying in a vacuum oven).

By using a lookup table for the vacuum capacitance of the recessed specimen inside the test cell (generated with a numerical field simulation) and the determined value of $C_{0,S}$, it is possible to noninvasively determine the electrode separation. This in turn provides information about the electric field amplitudes inside a specimen during an aging or breakdown experiment for a given applied voltage.

B. Specimens

In this paper, two different specimen geometries have been used (see Fig. 2). The conventional disc-shaped specimens are used for comparative performance assessments with commercial spectrometers as well as for determining the absolute value of a material's permittivity at one selected frequency and temperature (see previous section). The recessed specimens are intended for later use in voltage endurance and aging experiments under PWM high-voltage stressing. Two cylindrical aluminum electrodes (Ø 16 mm) with semispherical endings spaced between ~100 µm and ~1 mm are molded into an unfilled thermal class H high-voltage impregnation epoxy resin (Damisol 3418, Von Roll, T_g=136 °C).

C. Three-Electrode Test Cell

The test cell together with the insert for measuring disc-shaped specimens is shown in Fig. 2 (thermal insulation of cell is removed). Both the metallic cylinder (and guard ring for the parallel plate geometry) and the lower center electrode of the test cell ③ are at ground potential while only the current flowing between the high-potential and the center electrode is amplified and measured. In the parallel plate geometry ④a the electrodes are pressed against the sample surface by a three-point spring force, ensuring constant contact pressure when the sample volume expands/contracts due to temperature changes.

A thermostat ⑤ (Lauda KS6 and DLK 10) makes a silicone fluid circulate in ducts inside the cylinder wall. The temperature is adjustable from 20 °C to 150 °C with a nominal fluid bath temperature stability of 0.01 °C.

D. Graphical User Interface

The whole setup is remote controllable from a graphical user interface (GUI) ⑩ programmed in MATLAB®. Frequency and temperature scans can be run fully automatically from a predefined measurement protocol. Signal inspection, processing and result export is also done within the GUI. Additionally, the GUI includes a simulation panel where the influence of various parameters (such as vertical and horizontal ADC resolution, number of averages N, noise floor) can be investigated.

III. Results

A. Benchmark Measurements

For assessing the absolute accuracy of the setup, the reference dielectric polytetrafluoroethylene (PTFE) was chosen because of its well-known and stable dielectric properties. The measured magnitude and phase of its complex relative permittivity are shown in Fig. 3.

The measured spectrum for the epoxy polymer Damisol 3418 was compared with measurements done with a commercial high-end dielectric spectrometer (Novocontrol Alpha-A Analyzer, abbr. NCA) and a general-purpose impedance analyzer (Agilent 4980A, abbr. A4980) with a dielectric spectroscopy test fixture (Agilent 16451B). Due to instrument/sample holder constraints, different specimen thicknesses/vacuum capacitances were used: (0.4±0.01) mm/26 pF, (3.94±0.03) mm/2.5 pF and (3.94±0.03) mm/0.7 pF for the NCA, the A4980 and our setup, respectively. The loss spectra are shown in Fig. 4. The measured permittivity magnitude at 1 kHz was about 4% higher in comparison to the NCA, while the A4980 reported a 15% lower value compared to the latter.

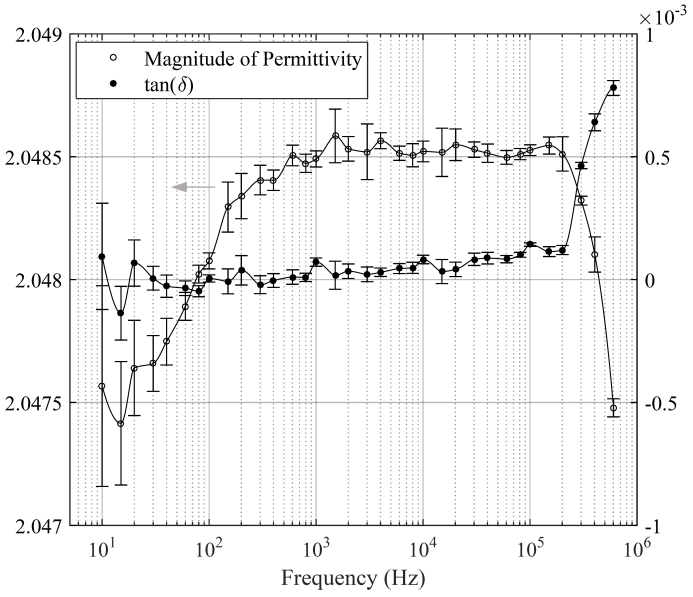

Fig. 3. Magnitude and loss factor of the complex relative permittivity of a (3.48±0.03) mm thick disc of PTFE (23 °C, vacuum capacitance 0.7 pF) measured with the setup to assess its accuracy and precision.

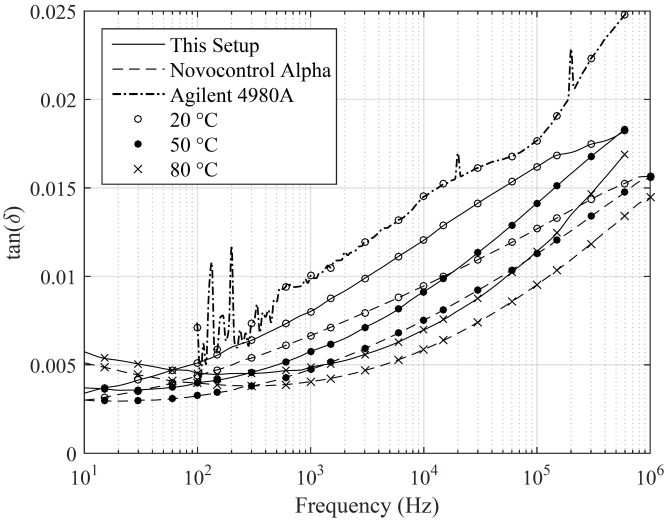

Fig. 4. Dielectric loss spectra of an unfilled epoxy polymer measured with three different instruments. Samples with different diameters and capacitances were used (see main text).

B. Precision

Using N=25 averages (single periods), the loss factor tan(δ) can be resolved with a precision of about $5 \cdot 10^{-5}$ over the bulk of the frequency range (see confidence intervals in Fig. 3) and is thus of the same order of magnitude as the nominal accuracy of the NCA ($3 \cdot 10^{-5}$). Exceptions are the lowest frequencies where sample current amplitudes are below ~100 nA and the signal-to-noise ratio is smaller. If desired the precision can be increased to that of the high-frequency level by choosing $N \approx 100$ in this range. The relative precision of the magnitude is very similar to the one of the phase. One notes that for the measured specimen capacitance of 1.6 pF (PTFE) this corresponds to a capacitance *resolution* of about 0.1 fF. The measurements with the A4980 are subject to strong noise below 1 kHz and no meaningful results could be obtained below 100 Hz.

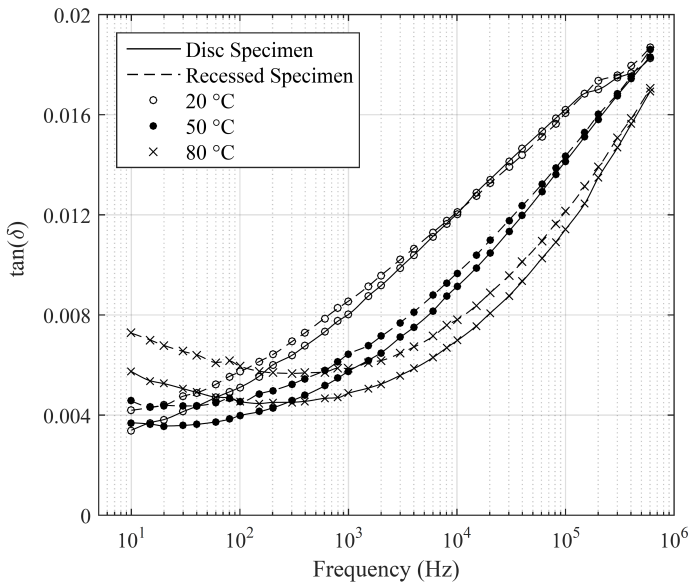

Fig. 5. Comparison of loss factor spectra for a disc-shaped sample and a recessed specimen (see Fig. 2) for an unfilled epoxy polymer.

The confidence intervals shown in Fig. 3 are robust, in the sense that consecutive measurements under the same conditions yield results that are not significantly different (except for the 5% expected for a 95% confidence interval). For the magnitude of the permittivity, small albeit significant changes are typically obtained after reinserting the specimen. This does not invalidate the confidence intervals, because relative capacitance changes of the order of ~100 ppm are to be expected when repositioning the sample.

C. Sample Geometry

A comparison between the loss factor measured for the same material (Damisol 3480) but two different sample geometries ④a/b is given in Fig. 5. The disc-shaped specimen was again (3.94±0.03) mm thick and of vacuum capacitance 0.7 pF. The electrode separation for the recessed specimen was determined to (0.91±0.03) mm with the method explained at the end of section II.A, corresponding to a vacuum capacitance of 0.8 pF inside the test cell.

There exists a small but highly significant difference between the loss factors of the two measured samples. It depends on both frequency and temperature, with a diverging tendency towards lower frequencies and higher temperatures.

D. Nonlinear Analog Signal Transfer

Specimen and reference capacitance can only approximately be matched for a frequency scan. Linearity of the signal conditioning and acquisition stage is thus a necessary assumption for the validity of (3). It is instructive to test this assumption by examining the transfer behavior of the signal transimpedance amplification, anti-aliasing filtering and ADC stage.

The initially chosen anti-aliasing filters (switched-capacitor type, 0.1 Hz<f_c<100 kHz) turned out to be unsuitable because they showed strong nonlinear behavior well below f_c and additionally increased the noise floor of the setup, thus compromising both the usable bandwidth and the precision of the setup. All measurements reported here were thus done without these filters. Fig. 6 depicts the phase of the transfer functions resulting from applying a sinusoidal signal of 1 V_{pp} and 10 V_{pp}, respectively, to a 1 MΩ through-hole resistor (metal film, 0.25 W) mounted into a coaxial housing and feeding the resulting current to the transimpedance amplifier (with the gain set to 10^6 V/A). In this scenario, significant nonlinear behavior is observed above f_c/10, where f_c=200 kHz is the -3 dB cutoff frequency of the chosen gain stage. The gain difference (locally) peaks at about f_c.

IV. Discussion

The measured dielectric properties of PTFE (Fig. 3) agree well with the ones reported in literature, which are tan(δ)<10^{-4} in the considered frequency range, and an approximately constant magnitude |ε| of a value between 2 and 2.1 [9]. The expected relative magnitude accuracy of 1% to 2% − mainly

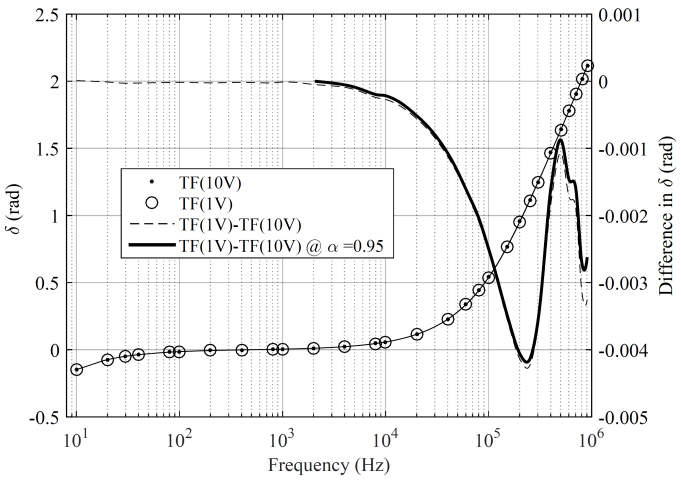

Fig. 6. Nonlinear phase transfer in the analog signal chain.

determined by the nominal accuracy of the transimpedance gain and the error on sample thickness measurement − could thus be confirmed. Based on this measurement, absolute loss factor accuracy is estimated to 10^{-4}, only slightly higher than the corresponding precision. Obvious departures from this basic loss factor accuracy are observed above 200 kHz. These seem to be related to significant system nonlinearities around its cutoff frequency (see below).

The differences in the loss spectra between the NCA and our setup (Fig. 4) are most likely attributable to different sample conditioning before measurement. The NCA started measurements at 170 °C (N_2 atmosphere) on freshly produced specimens, while the samples measured in our setup were stored for about 6 months prior to measurement (because the use of this epoxy polymer for recessed specimens was discontinued). The measurements of the A4980 were done on the same samples as in our setup and also show higher losses. Concerning the results of the A4980 it must be underlined that this device is not intended for precision measurements on capacitance values in the pF range at frequencies ≤10 kHz.

For a conclusive explanation of the observed difference between the disc-shaped and recessed specimen (Fig. 5) more in-depth measurements are necessary (excluding any possibility of differences in the polymer through differing manufacturing and storage conditions). Only then explanations based on non-uniform polarization densities within the dielectric can be put forward on firm ground.

As mentioned above, significant deviations from the basic loss factor accuracy occur above 200 kHz (see Fig. 3). They are observed to increase with an increasing mismatch between the specimen and the reference capacitance. This points to system nonlinearities as being at the origin of these deviations. Significant nonlinearities in the transfer function of an ohmic load could indeed be measured (Fig. 6). Since the nonlinear behavior is clearly linked to the value of the cutoff frequency of the chosen gain stage of the transimpedance amplifier, it is very likely that the nonlinearity originates in the latter. As precision rather than accuracy is the relevant figure of merit for aging studies, these systematic deviations do not compromise the usefulness of the setup for its intended applications.

V. Conclusion

A dielectric spectrometer adapted to precise measurements of the complex dielectric permittivity of low-capacitance recessed polymeric specimens has been realized and its functionality validated by benchmark measurements. The established precision of $\leq 10^{-4}$ in loss factor measurements and a relative precision of the same order of magnitude on capacitance measurements will allow sensitive offline aging diagnostics under harmonic excitation. The measurement frequency range is limited by a deteriorating signal-to-noise ratio at low frequencies and by amplifier bandwidth at high frequencies. For a specimen capacitance of ~1 pF the accessible frequencies range from ~10 Hz to ~600 kHz.

In a next step, multi-frequency excitations will be investigated and possible adaptations of the setup explored, which could make it operable in the MV test bench such that online monitoring of pre-breakdown degradation processes could be realized.

Acknowledgment

This work is part of the Swiss Competence Centers for Energy Research (SCCER-FURIES) initiative which is supported by the Swiss Commission for Technology and Innovation (CTI).

R.F. received the IEEE DEIS graduate fellowship for his proposal to carry out the research reported in this contribution.

We would like to thank the Polymer and Soft Matter Group at the Material Physics Center in San Sebastián, Spain, for the measurements with the Novocontrol Alpha-A analyzer.

Baumann Springs Ltd. and Von Roll Ltd. are gratefully acknowledged for their support in manufacturing materials, and the Power Electronic Systems Laboratory (PES) at ETH for placing at our disposal the Agilent 16451B.

References

[1] J. Biela, M. Schweizer, S. Waffler, and J.W. Kolar, "SiC versus Si – Evaluation of Potentials for Performance Improvement of Inverter and DC-DC Converter Systems by SiC Power Semiconductors," *IEEE Trans. Ind. Electron.,* vol. 58, no. 7, 2011.

[2] X.-P. Zhang, L. Yao, B. Chong, C. Sasse, K.R. Godfrey, "FACTS and HVDC technologies for the development of future power systems," *2005 Intern. Conf. on Future Power Systems,* 2005.

[3] T. Guillod, et al., "Characterization of the voltage and electric field stresses in multi-cell solid-state transformers," *IEEE Energy Conv. Congress and Exposition (ECCE),* 2014.

[4] T. Bengtsson, et al., "Repetitive Fast Voltage Stresses – Causes and Effects," *IEEE Elect. Insul. Mag.,* 2009.

[5] P. Wang, A. Cavallini, and G.C. Montanari, "The Influence of Repetitive Square Wave Voltage Parameters on Enameled Wire Endurance," *IEEE Trans. Dielectr. Electr. Insul.,* vol. 21, no. 3, 2014.

[6] T. Koltunowicz, A. Cavallini, D. Djairam, G.C. Montanari, and J. Smit, "The influence of square voltage waveforms on transformer insulation breakdown voltage," *Conf. on El. Insul. and Diel. Phen. (CEIDP)*, 2011.

[7] B. Sonerud, T. Bengtsson, J. Blennow, and S.M. Gubanski, "Dielectric Heating in Insulating Materials Subjected to Voltage Waveforms with High Harmonic Content," *IEEE Trans. Dielectr. Electr. Insul.,* vol. 16, no. 4, 2009.

[8] B. Sonerud, T. Bengtsson, J. Blennow, and S.M. Gubanski, "Dielectric Response Measurements Utilizing Semi-Square Voltage Waveforms," *IEEE Trans. Dielectr. Electr. Insul.,* vol. 15, no. 4, 2008.

[9] P. Ehrlich, "Dielectric Properties of Teflon from Room Temperature to 314°C and from Freqeuencies of 10^2 to 10^5 c/s," *Journal of Research of the National Bureau of Standards.,* vol. 51, no. 4, 1953.